ACCOUNTS of chemical research

Article

pubs.acs.org/accounts

Nonstoichiometric Nucleation and Growth of Multicomponent Nanocrystals in Solution

Yuho Min, Junghyeok Kwak, Aloysius Soon, and Unyong Jeong*

Department of Materials Science and Engineering, Yonsei University, 134 Shinchon-dong, Seoul 120-749, Korea

CONSPECTUS: The ability to assemble nanoscale functional building blocks is a useful and modular way for scientists to design valuable materials with specific physical and chemical properties. Chemists expect multicomponent, heterostructured nanocrystals to show unique electrical, thermal, and optical properties not seen in homogeneous, single-phase nanocrystals. Although researchers have made remarkable advances in heterogeneous nucleation and growth, design of synthetic conditions for obtaining nanocrystals with a target composition and shape is still a big challenge.

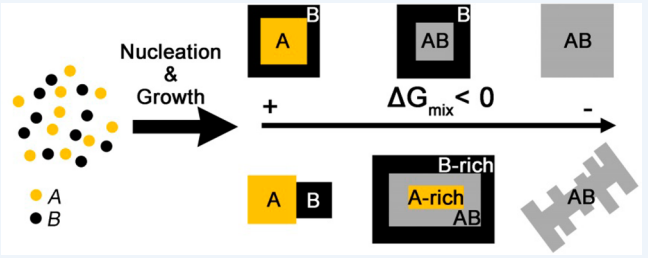

There are several outstanding issues that chemists need to address before they can successfully carry out the design-based synthesis of multicomponent nanocrystals. For instance, small changes in the reaction parameters, such as the precursor, solvent, surfactant, reducing agent, and the reaction temperature, often result in changes in the structure and chemical composition of the final product. Although scientists do not fully understand the mechanisms underlying the nucleation and growth processes involved in the synthesis of these multicomponent nanocrystals, recent progress in understanding of the thermodynamic and kinetic factors have improved our control over their final structure and chemical composition. In this Account, we summarize our recent advances in understanding of the nucleation and growth mechanisms involved in the solution-based synthesis of multicomponent nanocrystals. We also discuss the various challenges encountered in their synthesis, emphasizing what still needs special consideration.

We first discuss the three different nucleation paths from a thermodynamics perspective: amorphous nucleation, crystalline nucleation, and two-step nucleation. Amorphous nucleation and two-step nucleation involve the generation of nonstoichiometric nuclei. We initiate this process mainly by introducing an imbalance in the concentrations of the reduced elements. When the nonstoichiometric nuclei grow, we can add secondary elements to the growing nonstoichiometric nuclei. This leads to either the physical deposition or atomic mixture formation through the diffusion and rearrangement of constituents.

The processes of mixture formation and the physical deposition of the secondary constituent element also compete and determine the shape and chemical composition of the final product. If the free energy change by mixture formation is positive ($\Delta G_{AB} \geq 0$), physical deposition takes place predominantly, and the spreading coefficient (S) determines the structure of the nanocrystals. However, when mixture formation is highly spontaneous ($\Delta G_{AB} < -\xi$), the chemical composition of the final product is usually stoichiometric, and its shape then depends on the size of the primary nanocrystals. When the mixture formation and physical deposition are in competition ($-\xi \leq \Delta G_{AB} < 0$), as commonly seen for many nanoalloy systems, both the chemical composition and the structure are determined by the size of the primary nanocrystals as well as the degree of mixture formation at the interface of the constituent components. Finally, we discuss the challenges and caveats that one needs to take into account when synthesizing multicomponent nanocrystals.

1. INTRODUCTION

Methods for controlling the dimensions, shape, and elemental distribution of multicomponent nanocrystals have been explored extensively, as these parameters determine the physical and chemical properties of the nanocrystals.[1,2] Heterostructured nanocrystals are expected to exhibit electrical, thermal, and optical properties that are not obtained in homogeneous, single-phase nanocrystals.[3] Recently, remarkable advances have been made in the explicit control of structure and elemental distribution of multicomponent nanocrystals via heterogeneous stepwise synthetic approaches including epitaxy,[4] seeded growth,[5] and chemical transformation.[6] However, the design of the synthesis of nanocrystals with a particular target composition and shape, especially in homogeneous nucleation and growth, is still a great challenge. It is known that small changes in the reaction parameters (e.g., the precursor, solvent, surfactant, reducing agent, reaction temperature) may promote a different reaction pathway.[7] Thus, a firm understanding of the thermodynamic and kinetic factors in relation to the reaction pathways is required to improve the nanoscale control of the structures and elemental distribution.

Recent studies suggest that the nucleation stage may be a complicated process involving a two-step mechanism, and this may not be well described by the simple conventional nucleation theory.[8] The dynamic changes in the relative

Received: March 26, 2014
Published: August 18, 2014

   dx.doi.org/10.1021/ar500133w | Acc. Chem. Res. 2014, 47, 2887−2893

supersaturation of the constituent atoms during the synthesis point to the possibility of nonstoichiometric nucleation and growth. Many studies have suggested that the free energy of mixing in multicomponent systems plays a pivotal role in determining the final shape of nanocrystals grown from the nonstoichiometric nuclei.[9] However, there have been many experimental observations that cannot be clearly explained by this thermodynamic criterion.[2] It is, thus, the aim of this Account to highlight the recent progress made in elucidating the nucleation steps and the growth of nanocrystals in multicomponent systems. In addition, we will discuss the synthetic issues in lack of understanding. We focus on coreduction systems as the concepts can be readily extended to other synthetic approaches.

2. NUCLEATION OF SINGLE-ELEMENT NANOCRYSTALS

The nucleation and growth model proposed by Gibbs defines a critical size (R_a*) and a critical free energy (ΔG_a*) of a liquid precipitate (Figure 1A,B).[10] At the size larger than R_a*, stable

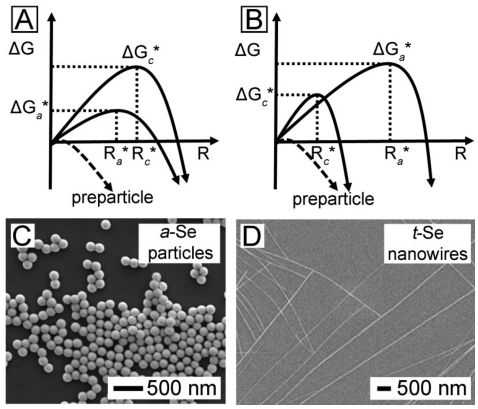

Figure 1. Nucleation of single-element nanocrystals. (A,B) Free energy changes (ΔG) of crystalline nucleus, amorphous nucleus, and preparticle aggregate as a function of the radius of nuclei. The reaction pathway differs according to the relative critical energy barrier of amorphous nuclei (ΔG_a*) and crystalline nuclei (ΔG_c*): (A) ΔG_a* < ΔG_c* and (B) ΔG_a* > ΔG_c*. (C) Synthesis of spherical amorphous selenium (*a*-Se) particles through the metastable amorphous nucleation path. (D) Physical transformation of the a-Se particles into crystalline nanowires. Panels (A) and (B) adapted from ref 10 with permission. Copyright 2013 Nature publishing Group. Panel (C) reprinted with permission from ref 11. Copyright 2008 American Chemical Society. Panel (D) reprinted from ref 12 with permission. Copyright 2009 Royal Society of Chemistry.

nuclei grow spontaneously. This classical model has been adopted extensively to describe the formation of crystalline nuclei by using the same concepts of the critical size (R_c*) and the critical energy barrier (ΔG_c*). In this classical model, nucleation and growth are proceeded by the consecutive deposition of atoms or molecules from a supersaturated solution. When ΔG_a* < ΔG_c* (Figure 1A), metastable amorphous nuclei may grow into large amorphous precipitates. For instance, uniform-sized submicrometer amorphous Se (*a*-Se) particles were obtained at room temperature synthesis (Figure 1C).[11] The metastable *a*-Se particles transformed into crystalline Se nanowires on annealing at 100 °C in a polymer liquid thin film (Figure 1D).[12] Such physical transition from an amorphous to a crystal has been often reported in the materials with long complex molecular configurations (like a polymer) as they often possess a large activation energy for crystallization.[13] For the case when ΔG_a* > ΔG_c* (Figure 1B), crystalline nuclei form and grow into stable nanocrystals.[14] The majority of metal nanocrystals are considered to follow this nucleation pathway.

Recently, it has been demonstrated that the final nanocrystals could be formed by the aggregation of kinetically favored metastable phases (clusters, preparticles) in random or oriented attachment.[14] These synthetic routes are referred to as the two-step nucleation process.[15] The preparticles form quickly when their critical free energy is negligible (dashed line in Figure 1A,B),[16] and are usually in an intermediate amorphous state which will eventually transform into the final crystalline product. Density functional theory based calculations indicate that the transition from an amorphous preparticle to a nanocrystal requires additional thermodynamic energy for atomic rearrangement involved. Such a phase transition can be the rate-determining step in the nanocrystal synthesis.[16,17] If this step is slow, the amorphous precipitate may evolve into a metastable amorphous sphere. In case where the preparticles are already crystalline, oriented attachment of these preparticles may take place to form stable crystals.[18] The detailed nucleation kinetics in the two-step mechanism have been well discussed in a recent review paper.[16]

3. NUCLEATION IN A COREDUCTION PROCESS

According to the extended form of the classical nucleation model, in the case of a spherical structure with a radius, R, the equilibrium partitioning of the individual components occurs under particular conditions. The total Gibbs free energy of the multicomponent nuclei is the sum of the two terms. That is, $\Delta G(\mu_i, R) = 4/3\pi R^3 \Delta G_{mix}(\mu_i) + 4\pi R^2 \gamma(\mu_i)$, where $\gamma(\mu_i)$ is the specific surface energy of the individual components. The free energy change of mixture formation, ΔG_{mix}, which is $G_{AB} - (\Delta G_A + \Delta G_B)$, is a thermodynamic driving force that results in the formation of a compound instead of the pure material A or B. The critical nucleation radius (R*) and the chemical composition can be determined by minimizing ΔG with respect to the nuclei radius, R, and the chemical potential of the individual components, μ_i, respectively.[19] This classical model assumes a stoichiometric elemental distribution in the whole process of nucleation and growth.[8] However, during the actual synthesis process, the relative degrees of supersaturation of the constituent elements vary with the synthesis time. This time-dependent elemental concentration makes it difficult to predict the structure and elemental distribution of nanocrystals. Furthermore, the relative ratio of the elemental concentrations is not linearly proportional to the precipitation rates of the atoms because the equilibrium concentrations (C_0) of the elements are different, $(C_B/C_A) = (C_{B,0}/C_{A,0})((1 + \sigma_B)/(1 + \sigma_A))$. It leads to different supersaturations (σ) even when the starting concentrations of the precursors are stoichiometric. If one element can form amorphous clusters or preparticles, the possibility to form nonstoichiometric nuclei increases more.

Figure 2A is a schematic energy diagram describing the chemical reduction of precursors (A') and the nucleation of the reduced atoms (A) in a binary system (A, B), where $\Delta G_A = G_A - G_{A'}$. From a thermodynamics perspective, if $\Delta G_A < \Delta G_B$, the precursor A' has a higher probability to be reduced faster than B' ; hence, the concentration of element A is expected to be higher than element B. If the elemental mass corresponding to equilibrium concentration C_0 is negligible compared to the total amount of the element used in the synthesis, the relative

dx.doi.org/10.1021/ar500133w | Acc. Chem. Res. 2014, 47, 2887−2893

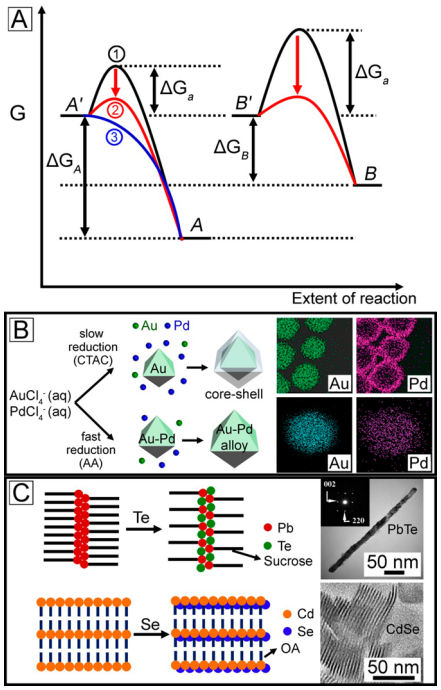

Figure 2. Nucleation during coreduction in a binary system. (A) Schematic plot of the change in the Gibbs free energies (ΔG_A, ΔG_B) and the activation energy (ΔG_a) during the conversion of the precursors (A', B') to the reduced elements (A, B). (B) Structural evolution of Au@Pd core−shell nanocrystals through reduction with cetyltrimethylammonium chloride (CTAC) and the evolution of Au−Pd alloy nanocrystals through reduction with L-ascorbic acid (AA) during the coreduction of $AuCl_4^-$ and $PdCl_4^-$. With permission, the core−shell nanocrystals were reproduced from ref 20 (copyright 2009 American Chemical Society) and the alloy nanocrystals from ref 21 (copyright 2011 WILEY VCH). (C) Schematic of the template-based approach initiated by the self-assembly of an organic-metal complex, and examples of nanostructures synthesized using this approach (PbTe nanowires and CdSe nanosheets). With permission, the PbTe nanowires are reproduced from ref 24 (copyright 2008 American Chemical Society) and the CdSe nanosheets from ref 25 (copyright 2009 WILEY VCH).

concentration (C_A/C_B) can be approximated to the relative supersaturation, namely, $C_A/C_B \approx \sigma_A/\sigma_B$. The value of C_A/C_B can then be estimated from the Boltzmann distribution relation, which is $C_A/C_B = K(T)\exp(-(\Delta G_A - \Delta G_B)/kT)$. On the basis of this argument, using precursors with the similar free energy change (ΔG) under the reaction condition can help the production of stoichiometric nanocrystals.

The reduction potential, E, is often used to estimate the spontaneity of a reduction process.[7] The reduction potential is the electromotive force for reduction at a certain concentration and temperature. That is, $E = -(\Delta G/nF)$, where n and F are the number of electrons involved in the reaction and Faraday's constant, respectively. A positive E leads to a spontaneous reduction reaction. A large difference in the reduction potentials ($E_A \gg E_B$) may cause a severe imbalance in the elemental concentrations. When the standard reduction potential (E°) of a precursor is used, several caveats should be kept in mind. First, the n value for the thermodynamic driving force (ΔG) should be considered. For example, the E° values for Ag^+/Ag and Bi^{3+}/Bi are 0.80 and 0.31 V, respectively. However, their standard Gibbs free energy differences (ΔG°) are -0.80×10^2 and -0.93×10^2 kJ/mol, respectively. This indicates that the reduction of Bi^{3+}/Bi is favored more than that of Ag^+/Ag. Second, the Nernst equation ($E = E^\circ - (RT/nF)\ln Q$) indicates that the actual reduction potential depends on the reaction temperature and the concentrations of the chemicals involved in the reaction. It should be noted that the reduction potential is not simply an intrinsic property of the elements or chemical compounds, but rather a property of the solution under a specific condition. Third, the E° values correspond to aqueous solutions at room temperature. Therefore, using the values may be questionable in many reactions taking place in nonpolar solvents or at high temperatures. Fourthly, when the reduction involves H^+ or OH^-, the E value is also affected by pH level. For example, in the reaction $TeO_3^{2-} + 6H^+ + 4e^- \rightarrow Te_{(s)} + 3H_2O$, E can be expressed as $E = E^\circ - (RT/4F)(\ln[TeO_3^{2-}] - 2.3\ \mathrm{pH})$. Therefore, a change in the pH level induced by additives or surfactants can result in different reduction kinetics.

When the reduction rates of the precursors are high, the elemental distribution and structure of the nuclei are governed mainly by the reduction kinetics. The activation energy (ΔG_a) for reduction is expressed by the Arrhenius equation, $\Delta G_a = RT^2(\mathrm{d}\ln k/\mathrm{d}T)$. A high activation energy of precursor B' results in a low reduction rate than A' (case 1 in Figure 2A). The pre-exponential factor in the Arrhenius equation is proportional to $T^{1/2}$ if one does not consider the steric factor between the precursors and the reducing agents, which infers that the activation energy can be reduced simply by increasing the reaction temperature (case 2 in Figure 2A).[8] Another way of decreasing the activation energy is through the formation of an intermediate complex. Figure 2B shows an example of controlling the structure obtained by adjusting the activation energy. When $AuCl_4^-$ and $PdCl_4^-$ were reduced in water using a weak reducing agent, cetyltrimethylammonium chloride (CTAC), Au nanocrystals grew initially, and Pd formed a shell through epitaxial growth on the Au core.[20] This process was driven by the difference in the reduction potentials of $AuCl_4^-/Au$ (E° = 1.002 V) and $PdCl_4^-/Pd$ (E° = 0.591 V). When the reducing power was increased by adding L-ascorbic acid (AA), Au−Pd alloy nanocrystals were obtained under identical reaction conditions.[21] This change is caused by a decrease of the activation energy (red line in Figure 2A), which increases the reduction rate of Pd even though the reduction potential is not favorable.

Recent simulation studies rationalize that stable clusters can be formed below the critical supersaturation level when the constituent elements have high attraction energies such as hydrogen bonds.[22] During the synthesis of inorganic nanocrystals, an organic surfactant can help decrease the surface energy of the clusters. Therefore, the critical size of the nuclei (R^*) can be much smaller than that expected in the case of clean crystal surfaces. The spontaneous nucleation of nanocrystals with almost zero activation energy was reported in the synthesis using ligands with specific binding energies (case 3 in Figure 2A).[23] The molecular complex between the surfactant and element self-assembled and created inorganic clusters of the element. These assembled structures acted as a template for the subsequent deposition of the constituent elements. The clusters grew into nanocrystals through the alternating deposition of the elements from within the template. This template-based approach can be an effective way of producing ultrathin anisotropic nanocrystals. Figure 2C show images of PbTe nanowires[24] and CdSe nanosheets[25] synthesized by this template-based approach. The exclusive interaction of the

dx.doi.org/10.1021/ar500133w | Acc. Chem. Res. 2014, 47, 2887−2893

hydroxyl groups in sucrose with Pb caused a strong complex that assembled into a one-dimensional template. Similarly, a cadmium chloride octylamine $[CdCl_2(OA)_2]$ complex created a repeated lamellar structure owing to the van der Waals attraction between the hydrocarbon side chains of octylamine. The incorporation of Se into this two-dimensional (2D) template produced a stack of CdSe nanosheets. The assembly of the complex started with one elemental species and it continued even when the concentration of the other element is still very low, suggesting that stoichiometry was not critical in the template-based synthesis.

4. GROWTH OF NONSTOICHIOMETRIC NUCLEI IN A COREDUCTION PROCESS

Once a nonstoichiometric nucleus (pure *A* or *A*-rich) is formed in a binary system (*A*, *B*), the nucleus should grow in an *A*-rich solution through a *B*-rich solution. Hence, the elemental distribution and structure of the nucleus continue to vary as it grows. Because this Account considers only nanosized crystals, the possibility of incomplete transformation owing to the thick diffusion barrier in submicrometer particles was not considered. Although the formation of alloy or compound is preferred at high pressure, the pressure in most solvothermal and hydrothermal reactions is negligible. On the basis of these arguments, we categorized the growth of nuclei according to the ΔG_{mix} values as followings.

4.1. Physical Deposition of Secondary Elements ($\Delta G_{mix} \geq 0$)

When $\Delta G_{mix} \geq 0$, as is typically the case for semiconductor/metal or metal/metal phases, the structure of the nanocrystals is determined by the relative concentrations of the elements and the surface energies of the primary (*A*) and secondary (*B*) phases (Figure 3A).[2] The two phases form an inorganic interface (*AB*), which is accompanied by a change in the total surface free energy. The spreading coefficient (*S*), where $S = \gamma_A - (\gamma_B + \gamma_{AB})$ and γ_{AB} is an interfacial tension between component *A* and *B*, has been used widely to predict whether a liquid droplet will wet or dewet a solid surface.[26] If $S < 0$, phase *B* dewets partially or completely, and thus, dimerlike heterostructured nanocrystals are formed.[27,28] If $S > 0$, phase *B* wets the surface of phase *A* spontaneously, and thus, a core–shell structure or pancakelike structures are produced.[29]

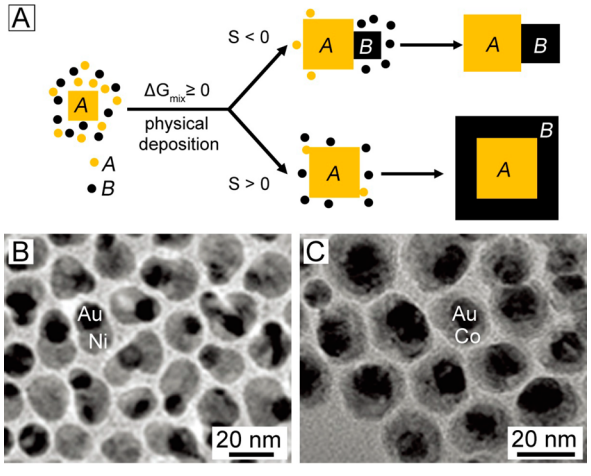

Figure 3. (A) Physical deposition of the secondary element (*B*) on a primary nanocrystal (*A*) under the condition $\Delta G_{mix} \geq 0$. Heterostructures and core–shell structures are formed by the dewetting ($S < 0$) and complete wetting ($S > 0$) of the secondary element (*B*), respectively. (B, C) Transmission electron microscopy (TEM) images of Au–Ni dimerlike nanocrystals (B) and Au@Co core–shell nanocrystals. Reprinted with permission from ref 32. Copyright 2010 American Chemical Society.

The concept of spreading coefficient is straightforward, but its application in solution-based synthesis often fails to predict the correct structure. If the elemental distribution in a growing nanocrystal is dynamic during the synthesis, the interfacial energy (γ_{AB}) changes continuously. Mutual diffusion of the elements between the phases, if it exists, increases with the reaction temperature, lowering the interfacial energy. Further, the degree of coherence in the crystallographic lattice affects the value of γ_{AB} significantly. A lattice mismatch results in a high γ_{AB}, while lattice matching leads to a low γ_{AB}. Therefore, the secondary phase nucleates epitaxially on the facets that exhibit a high degree of lattice matching. The γ_{AB} is an intrinsic value corresponding to the interface and is a function of temperature only. On the other hand, the surface energies (γ_A, γ_B) in a solution can be varied by changing the solvents or surfactants, in addition to the reaction temperature. The choice of the proper surfactant that binds selectively to the *A* or *B* phase can result in new heterostructures that are different from the ones predicted on the basis of the surface energies of the constituent materials in air. When the γ_A and γ_B are decreased significantly by surfactants, the γ_{AB} value may play a critical role in the development of heterostructures.

For instance, if Ni or Co is deposited onto Au surface in vacuum, they are expected to dewet because the surface energies of Ni (2450 ergs/cm^2) and Co (2550 ergs/cm^2) in air at their melting temperatures is much larger than that of the Au (111) surface (1610 ergs/cm^2).[30,31] As expected, Au–Ni dimerlike nanocrystals were synthesized in a solution phase by the coreduction of Au and Ni in the presence of octadecylamine (ODE) (Figure 3B).[32] Au was reduced first, then Ni was deposited on the Au surface. During this synthesis, the amine groups binding to the metal surface reduced both γ_A and γ_B significantly; however, the severe lattice mismatch caused γ_{AB} to be large, resulting in dewetting of Ni. On the other hand, Au@Co core–shell nanocrystals were obtained by coreduction in the presence of ODE (Figure 3C).[32] The quasi-perfect crystallographic matching between Co/Au (111) was considered to decrease γ_{AB} to be lower than that in the case of Ni–Au.[33] Transformations in structure, from core–shell nanocrystals into pancakelike nanocrystals, are often observed upon thermal annealing both in solution and in dry powder form.[34,35] This is caused by the disjoining pressure, which prevents the liquid shell layer from becoming too thin.[26] Such transformations can be an effective route for producing dimerlike nanocrystals or nanocrystals with spotted secondary phase on a primary phase.

The use of computer simulation and modeling has become a powerful approach to decipher nucleation and growth processes at the atomic level.[36,37] The composition-dependent transition from core–shell to quasi-Janus particles (as those shown in Figure 3A) was investigated by density functional theory (DFT) calculations and atomistic molecular dynamics simulations.[38] The calculations suggested that energetically favored subsurface Cu impurities in Ag nanoclusters act as seeds for the nucleation of off-center Cu nanoclusters, leading to the formation of quasi-Janus structures for Ag-rich compositions. The driving forces for the stabilization of off-center cores in *B*-rich metallic *A*/*B* nanoalloys have been discussed in refs 39 and 40. The key role of strain induced by lattice mismatch was also

dx.doi.org/10.1021/ar500133w | Acc. Chem. Res. 2014, 47, 2887–2893

clearly demonstrated in these works. Interestingly, in the phase-separated quasi-Janus configurations, it was predicted that a rather thin shell of the *B* element with a lower surface energy could coat the *A* element almost completely. In these works, the authors have demonstrated these effects over a series of weakly miscible nanoalloy systems, for example, Ag/Ni, Ag/Co, and Au/Co.[39,40] For the case of *A*-rich bimetallic systems, the driving force for the stabilization of symmetric core−shell nanoparticles was also discussed by the same authors.[41]

4.2. Alloy Formation ($\Delta G_{mix} < -\xi$)

If ΔG_{mix} is sufficiently small ($\Delta G_{mix} < -\xi$), where ξ is a large positive value, the chemical transformation of primary nanocrystals into an alloy or compound is spontaneous. Hence, the chemical composition of the resulting nanocrystals becomes stoichiometric in the end. This type of a reaction often occurs during the synthesis of metal chalcogenides. The structure of such nanocrystals is governed mainly by the size of the primary nanocrystals at the time the chemical transformation begins to occur (Figure 4A). When the primary nanocrystals are small, they are converted into seed alloy particles first and subsequently transformed into well-defined stoichiometric compound.

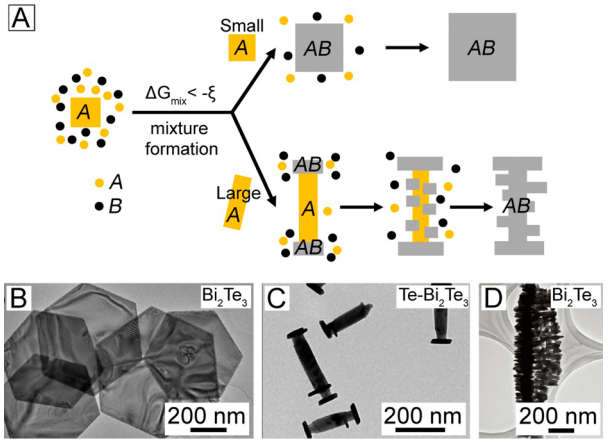

Figure 4. (A) Spontaneous alloy formation under the condition $\Delta G_{mix} < -\xi$, and the dependence of their structure on the size of the primary nanocrystals. (B−D) TEM images of single-crystalline Bi_2Te_3 nanoplates (B), barbell-shaped Te−Bi_2Te_3 heterostructures (C), and hierarchical Bi_2Te_3 nanocrystals consisting of a stack of Bi_2Te_3 nanoplates (D). Panels (B), (C), and (D) reprinted with permission from refs 42 (copyright 2013 American Chemical Society), 44 (copyright 2010 American Chemical Society), and 45 (copyright 2010 American Chemical Society), respectively.

In the case of Bi_2Te_3 nanocrystals, the compound formation between elemental Bi and Te is spontaneous, and the reaction rate is high. Although the standard reduction potential of TeO_3^{2-} is much higher than that of Bi^{3+}, a solvothermal reaction in an autoclave at 180 °C resulted in relative elemental concentrations similar to those suggested by stoichiometry. Hence, 2D Bi_2Te_3 nanoplates with well-defined crystalline facets could be obtained (Figure 4B).[42] If one element nucleates quickly and the other joins the reaction shortly after the primary crystals grow, the second element is doped on the facets of the crystals that exhibit a relatively high surface energy. The doping of the second element reduces the surface energy of the facets, which slows the growth of the primary nanocrystals.[43] By subsequent elemental supply and interdiffusion, heterogeneous nucleation of the compound occurs first on the surfaces with higher energies and then on the surfaces with lower energies. When the growth rate of the nuclei on the high-energy surfaces is greater than the nucleation rate on the lower-energy surfaces, the shape of the primary nanocrystals remains unchanged throughout the growth process. The reaction of TeO_3^{2-} and Bi^{3+} at 150 °C in the presence of hydrazine hydrate resulted in 1D Te nanorods, owing to the higher reduction rate of TeO_3^{2-}. Bi_2Te_3 nanoplates grew at the growth tips of Te nanorods, producing Te−Bi_2Te_3 nanosized barbells (Figure 4C).[44] The small lattice mismatch (1.62%) between Te (0001) and Bi_2Te_3 (0001) and the sharp curvature at the tips of the Te nanorods preferentially induced the epitaxial growth of Bi_2Te_3 nanoplates on the tips of the nanorods.[44] If the primary nanocrystals have already grown into large crystals, the heterogeneous nucleation takes place over the entire body of the primary nanocrystals, creating a large number of nuclei on the surfaces at the same time.[45] The growth of these nuclei produces stoichiometric compound nanocrystals. Te grew preferentially into large one-dimensional (1D) nanorods either when the reaction temperature was low or when the concentration of the reducing agent was low. The subsequent nucleation of the Bi_2Te_3 nanoplates took place on the side surfaces as well as on the growth tips of the Te nanorods. This resulted in a stack of Bi_2Te_3 nanoplates along the axial direction of the Te nanorods (Figure 4D).[45]

4.3. Physical Deposition versus Alloy Formation ($-\xi < \Delta G_{mix} < 0$)

If ΔG_{mix} is the intermediate range ($-\xi < \Delta G_{mix} < 0$), the physical deposition and alloy formation processes compete during nanocrystal growth. Hence, the elemental distribution and structure of the nanocrystals are sensitive to the synthesis conditions (Figure 5A). Because mixing of atoms is involved, the surface energies of the nanocrystals vary during the synthesis process. When the primary nanocrystal (*A*) is small, alloy formation may commence right at the beginning, producing nanoalloy seeds. The element *B* results in the coating of the surface of the nanoalloy seeds, producing an

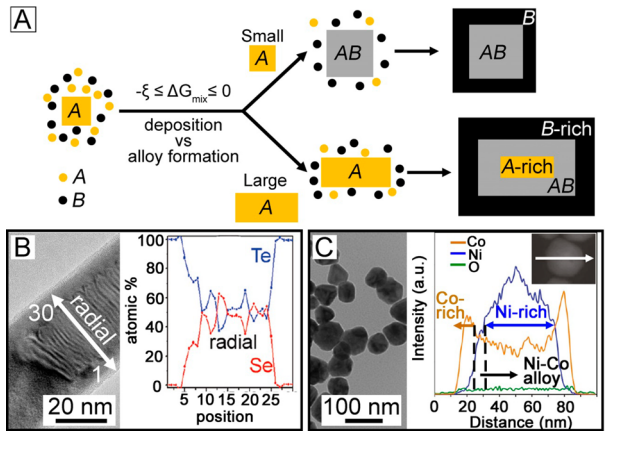

Figure 5. (A) Competition between physical deposition and alloy formation during the growth of nanocrystals under the condition $-\xi \leq \Delta G_{mix} \leq 0$. (B) TEM image and energy-dispersive X-ray spectroscopy line scan along the radial direction of the Se_xTe_y@Te nanorod. Reprinted with permission from ref 46. Copyright 2010 American Chemical Society. (C) TEM image and cross-sectional elemental profile of a single Ni@Ni−Co@Co nanoparticle. Reprinted with permission from ref 47. Copyright 2011 American Chemical Society.

dx.doi.org/10.1021/ar500133w | Acc. Chem. Res. 2014, 47, 2887−2893

AB@B core−shell structure. The elemental fraction of *B* increases gradiently near the core−shell interface, which is contrary to the sharp interface when $\Delta G_{mix} > 0$.

For example, elemental Se and Te are known to form a solid solution, owing to their high miscibility. The standard reduction potential of SeO_3^{2-} ($E^\circ = -0.36$ V) is higher than that of TeO_3^{2-} ($E^\circ = -0.42$ V) in a basic solution. This leads to the formation of Se-rich Se_xTe_y core. Subsequent deposition of Te results in Se_xTe_y@Te core−shell nanorods (Figure 5B).[46] When the primary nanocrystals are large and alloy formation is slow so that the conversion is limited to the surface area of the growing primary crystals, the elemental concentration of *B* in the growing nanocrystal increases gradually. This results in the production of *A@AB@B* nanocrystals. As another example, elemental Ni and Co has good miscibility, and they form an alloy in the liquid phase. Although the standard reduction potential of Co^{2+} ($E^\circ = -0.280$ V) is similar to that of Ni^{2+} ($E^\circ = -0.257$ V), reduction rates of the precursors became different in the presence of complexation agent, oleylamin. Ni^{2+} was reduced first, from the nickel(II) acetate-oleylamine complex at ∼110 °C, to form Ni nanocrystals.[47] The Ni nanocrystals act as a catalyst for the reduction of Co^{2+} in the cobalt(II) formate-oleylamine complex, resulting in the formation of heterostructured nanocrystals (Ni@Ni−Co@Co).[47]

5. CHALLENGES AND PERSPECTIVES

This Account summarizes the recent advances elucidating the nucleation and growth mechanisms involved in multicomponent nanocrystal synthesis. We have discussed the fundamental issues, namely, the formation of nonstoichiometric nuclei and the competition between the rates of alloy formation and physical deposition onto the nonstoichiometric nuclei. In addition to these issues, the activation energy for atomic rearrangement is seen as another key factor that could have a significant effect on final structure of the nanocrystals. When thermally annealed at sufficiently high temperatures, a physical transition takes place from the amorphous aggregates to crystals with well-developed facets. The oriented attachment of crystalline preparticles followed by atomic rearrangement to form large metal chalcogenide 2D nanocrystals is of intensive interest due to their unique electronic, thermoelectric, and topological insulating properties.[48−50]

This Account has discussed a few important caveats to keep in mind when considering solution-based synthesis of multicomponent nanocrystals. First, the standard reduction potentials used to estimate the spontaneity of reduction are calculated with respect to aqueous solutions at room temperature. Therefore, they must be used with caution when the reaction occurs at high temperatures or in nonpolar solvents. Second, the activation energies determining the reduction rates need to be investigated thoroughly. In particular, the effects of reaction temperature, complexing additives, surfactants, and solvents should be studied thoroughly. Third, the surface energies of nanocrystals in a solution can be completely different from their surface energies in vacuum because surfactants can selectively decrease the surface energies of individual nanocrystals. Therefore, decreases in the surface energies owing to the bonds between surfactants and elements should be taken into account. A clear understanding of these issues in binary systems is highly desired. If extended to complex systems, it could allow for the prediction-based synthesis of multicomponent nanocrystals.

AUTHOR INFORMATION

Corresponding Author

*E-mail: ujeong@yonsei.ac.kr.

Notes

The authors declare no competing financial interest.

Biographies

Yuho Min received a B.S. degree in the Department of Materials Science and Engineering from Yonsei University in 2010. He is pursuing his Ph.D. degree under the supervision of Prof. Unyong Jeong in the same department. His research interests include synthesis of metal chalcogenide nanomaterials and their thermoelectric applications.

Junghyeok Kwak received a B.S. degree in the Dept. of Materials Science and Engineering from Yonsei University in 2013. He is pursuing his Ph.D. degree under the supervision of Prof. Unyong Jeong in the same department. He tries to reveal the reaction kinetics of heterostructured nanocrystals.

Aloysius Soon holds a Ph.D. in Physics from the University of Sydney. He was an Alexander von Humboldt postdoctoral fellow at the Fritz-Haber-Institut der Max-Planck-Gesellschaft for two years, and joined the Department of Materials Science and Engineering at Yonsei University as an Assistant Professor in 2010. His research focuses on the development and application of materials theory and first-principles computational methods for the fundamental understanding of the chemistry and physics of materials.

Unyong Jeong received his Ph.D. in Chemical Engineering from POSTECH in Korea. He spent two years as a postdoctoral research associate at University of Washington. He moved to Materials Science and Engineering at Yonsei University in 2006 and now he is an associate professor. His research interest includes production of nanostructured materials, colloids, and fibers by electrohydrodynamics, and organic/inorganic hybrid materials for electronic devices.

ACKNOWLEDGMENTS

This work was supported by Samsung Research Funding Center of Samsung Electronics under Project Number SRFC-MA1301-07 and the National Research Foundation of Korea (NRF Grant No. 2014R1A1A1003415).

REFERENCES

(1) Burda, C.; Chen, X.; Narayanan, R.; El-Sayed, M. A. Chemistry and Properties of Nanocrystals of Different Shapes. *Chem. Rev.* **2005**, *105*, 1025−1102.

(2) Carbone, L.; Cozzoli, P. D. Colloidal Heterostructured Nanocrystals: Synthesis and Growth Mechanisms. *Nano Today* **2010**, *5*, 449−493.

(3) Talapin, D. V.; Lee, J.-S.; Kovalenko, M. V.; Shevhenko, E. V. Prospects of Colloidal Nanocrystals for Electronic and Optoelectronic Application. *Chem. Rev.* **2010**, *110*, 389−458.

(4) Fan, F.-R.; Liu, D.-Y.; Wu, Y.-F.; Duan, S.; Xie, Z.-X.; Jiang, Z.-Y.; Tian, Z.-Q. Epitaixal Growth of Heterogeneous Metal Nanocrystals: From Gold Nano-octahedra to Palladium and Silver Nanocubes. *J. Am. Chem. Soc.* **2008**, *130*, 6949−6951.

(5) Habas, S. E.; Lee, H.; Radmilovic, V.; Somorjai, G. A.; Yang, P. Shaping Binary Metal Nanocrystals through Epitaxial Seeded Growth. *Nat. Mater.* **2007**, *6*, 692−697.

(6) Moon, G. D.; Ko, S.; Xia, Y.; Jeong, U. Chemical Transformations in Ultrathin Chalcogenide Nanowires. *ACS Nano* **2010**, *4*, 2307−2319.

(7) Wang, D.; Li, Y. Bimetallic Nanocrystals: Liquid-Phase Synthesis and Catalytic Applications. *Adv. Mater.* **2011**, *23*, 1044−1060.

(8) Erdemir, D.; Lee, A. Y.; Myerson, A. S. Nucleation of Crystals from Solution: Classical and Two-Step Models. *Acc. Chem. Res.* **2009**, *40*, 621−629.
(9) Ferrando, R.; Jellinek, J.; Johnston, R. L. Nanoalloys: From Theory to Applications of Alloy Clusters and Nanoparticles. *Chem. Rev.* **2008**, *108*, 845−910.
(10) Baumgartner, J.; Dey, A.; Bomans, P. H. H.; Coadou, C. L.; Fratzl, P.; Sommerdijk, N. A. J. M.; Faivre, D. Nucleation and Growth of Magnetite from Solution. *Nat. Mater.* **2013**, *12*, 310−314.
(11) Moon, G. D.; Jeong, U. Decoration of the Interior Surface of Hollow Spherical Silica Colloids with Pt Nanoparticles. *Chem. Mater.* **2008**, *20*, 3003−3007.
(12) Ko, S.; Park, M.; Kee, J. S.; Kim, Y. S.; Ryu, D. Y.; Jeong, U. In-plane Growth and Directional Control of Se Nanowires in Polymer Thin Films. *Chem. Commun.* **2009**, 1855−1857.
(13) Galkin, O.; Pan, W.; Filobelo, L.; Hirsch, R. E.; Nagel, R. L.; Vekilov, P. G. Two-Step Mechanism of Homogeneous Nucleation of Sickle Cell Heomoglobin Polymers. *Biophys. J.* **2007**, *93*, 902−913.
(14) Yoreo, J. D. More than One Pathway. *Nat. Mater.* **2013**, *12*, 284−285.
(15) Myerson, A. S.; Trout, B. L. Nucleation from Solution. *Science* **2013**, *341*, 855−856.
(16) Vekilov, P. G. The Two-step Mechanism of Nucleation of Crystals in Solution. *Nanoscale* **2010**, *2*, 2346−2357.
(17) Chakraborty, D.; Patey, G. N. How Crystals Nucleate and Grow in Aqueous NaCl Solution. *J. Phys. Chem. Lett.* **2013**, *4*, 573−578.
(18) Niederberger, M.; Cölfen, H. Oriented Attachment and Mesocrystals: Non-classical Crystallization Mechanisms Based on Nanoparticle Assembly. *Phys. Chem. Chem. Phys.* **2006**, *8*, 3271−3287.
(19) Kashchiev, D.; van Rosmalen, G. M. Review: Nucleation in Solution Revisited. *Cryst. Res. Technol.* **2003**, *38*, 555−574.
(20) Lee, Y. W.; Kim, M.; Kim, Z. H.; Han, S. W. One-Step Synthesis of Au@Pd Core-Shell Nanooctahedron. *J. Am. Chem. Soc.* **2009**, *131*, 17036−17037.
(21) Hong, J. W.; Kim, D.; Lee, Y. W.; Kim, M.; Kang, S. W.; Han, S. W. Atomic-Distribution-Dependent Electrocatalytic Activity of Au-Pd Bimetallic Nanocrystals. *Angew. Chem., Int. Ed.* **2011**, *50*, 8876−8880.
(22) Hamad, S.; Moon, C.; Catlow, C. R. A.; Hulme, A. T.; Price, S. L. Kinetic Insights into the Role of the Solvent in the Polymorphism of 5-Fluorouracil from Molecular Dynamics Simulations. *J. Phys. Chem. B* **2006**, *110*, 3323−3329.
(23) Lifshitz, E.; Bashouti, M.; Kloper, V.; Kigel, A.; Eisen, M. S.; Berger, S. Synthesis and Characterization of PbSe Quantum Wires, Multipods, Quantum Rods, and Cubes. *Nano Lett.* **2003**, *3*, 857−862.
(24) Yan, Q.; Chen, H.; Zhou, W.; Hng, H. H.; Boey, F. Y. C.; Ma, J. A Simple Chemical Approach for PbTe Nanowires with Enhanced Thermoelectric Properties. *Chem. Mater.* **2008**, *20*, 6298−6300.
(25) Son, J. S.; Wen, X.-D.; Joo, J.; Chae, J.; Baek, S.-I.; Park, K.; Kim, J. H.; An, K.; Yu, J. H.; Kwon, S. G.; Choi, S.-H.; Wang, Z.; Kim, Y.-W.; Kuk, Y.; Hoffmann, R.; Hyeon, T. Large-Scale Soft Colloidal Template Synthesis of 1.4 nm Thick CdSe Nanosheets. *Angew. Chem., Int. Ed.* **2009**, *48*, 6861−6864.
(26) Brochard-Wyart, F.; Dimeglio, J.-M.; Quéré, D.; Degennes, P.-G. Spreading of Nonvolatile Liquids in a Continuum Picture. *Langmuir* **1991**, *7*, 335−338.
(27) Choi, S. H.; Kim, E. G.; Hyeon, T. One-Pot Synthesis of Copper-Indium Sulfide Nanocrystal Heterostructures with Acorn, Bottle, and Larva Shapes. *J. Am. Chem. Soc.* **2006**, *128*, 2520−2521.
(28) Figuerola, A.; Fiore, A.; Corato, R. D.; Falqui, A.; Giannini, C.; Micotti, E. One-Pot Synthesis and Characterization of Size-Controlled Bimagnetic FePt-iron Oxide Heterodimer Nanocrystals. *J. Am. Chem. Soc.* **2008**, *130*, 1477−1487.
(29) Reiss, P.; Protière, M.; Li, L. Core/Shell Semiconductor Nanocrystals. *Small* **2009**, *5*, 154−168.
(30) Boer, F. R.; Boom, R.; Mattens, W. C. M.; Miedema, A. R.; Niessen, A. K. *Cohesion in Metals: Transition Metal Alloys*; North-Holland: Amsterdam, Oxford, New York, Tokyo, 1988.
(31) Skriver, H. L.; Rosengaard, N. M. Surface Energy and Work Function of Elemental Metals. *Phys. Rev. B* **1992**, *46*, 7157−7168.
(32) Wang, D.; Li, Y. One-Pot Protocol for Au-Based Hybrid Magnetic Nanostructures via a Noble Metal-Induced Reduction Process. *J. Am. Chem. Soc.* **2010**, *132*, 6280−6281.
(33) Marsot, N.; Belkhou, R.; Magnan, H.; Le Févre, P.; Guillot, C.; Chandesris, D. Structure and Local Order in Co Magnetic Thin Films on Au(111): A Surface EXAFS Study. *Phys. Rev. B* **1999**, *59*, 3135−3141.
(34) Yang, Y.; Yang, R. B.; Fan, H. J.; Scholz, R.; Huang, Z.; Berger, A.; Qin, Y.; Knez, M.; Gosele, U. Diffusion-Facilitated Fabrication of Gold-Decorated Zn_2SiO_4 Nanotubes by a One-Step Solid-State Reaction. *Angew. Chem., Int. Ed.* **2010**, *49*, 1442−1446.
(35) Lu, Y.; Xiong, H.; Jiang, X.; Xia, Y. Asymmetric Dimers Can Be Formed by Dewetting Half-Shells of Gold Deposited on the Surfaces of Spherical Oxide Colloids. *J. Am. Chem. Soc.* **2003**, *125*, 12724−12725.
(36) Gebauer, D.; Kellermeier, M.; Gale, J. D.; Bergström, L.; Cölfen, H. Pre-nucleation Clusters as Solute Precursors in Crystallisation. *Chem. Soc. Rev.* **2014**, *43*, 2348−2371.
(37) Panizon, E.; Bochicchio, D.; Rossi, G.; Ferrando, R. Tuning the Structure of Nanoparticles by Small Concentrations of Impurities. *Chem. Mater.* **2014**, *26*, 3354−3356.
(38) Langlois, C.; Li, Z. L.; Yuan, J.; Alloyeau, D.; Nelayah, J.; Bochicchio, D.; Ferrando, R.; Ricolleau, C. Transition from Core-shell to Janus Chemical Configuration for Bimetallic Nanoparticles. *Nanoscale* **2012**, *4*, 3381−3388.
(39) Bochicchio, D.; Ferrando, R. Morphological Instability of Core-shell Metallic Nanoparticles. *Phys. Rev. B* **2013**, *87*, 165435.
(40) Laasonen, K.; Panizon, E.; Bochicchio, D.; Ferrando, R. Competition between Icosahedral Motifs in AgCu, AgNi, and AgCo Nanoalloys: A Combined Atomistic-DFT Study. *J. Phys. Chem. C* **2013**, *117*, 26405−26413.
(41) Bochicchio, D.; Ferrando, R. Size-Dependent Transition to High-Symmetry Chiral Structures in AgCu, AgCo, AgNi, and AuNi Nanoalloys. *Nano Lett.* **2010**, *10*, 4211−4215.
(42) Zhang, Y.; Hu, L. P.; Zhu, T. J.; Xie, J.; Zhao, X. B. High Yield Bi_2Te_3 Single Crystal Nanosheets with Uniform Morphology via a Solvothermal Synthesis. *Cryst. Growth Des.* **2013**, *13*, 645−651.
(43) Erwin, S. C.; Zu, L.; Haftel, M. I.; Efros, A. L.; Kennedy, T. A.; Norris, D. J. Doping Semiconductor Nanocrystals. *Nature* **2005**, *436*, 91−94.
(44) Wang, W.; Goebl, J.; He, L.; Aloni, S.; Hu, Y.; Zhen, L.; Yin, Y. Epitaxial Growth of Shape-Controlled Bi_2Te_3-Te Heterogeneous Nanostructures. *J. Am. Chem. Soc.* **2010**, *132*, 17316−17324.
(45) Mi, J.-L.; Lock, N.; Sun, T.; Christensen, M.; Sondergaard, M.; Hald, P.; Hng, H. H.; Ma, J.; Iversen, B. B. Biomolecule-Assisted Hydrothermal Synthesis and Self-Assembly of Bi_2Te_3 Nanostring-Cluster Hierarchical Structure. *ACS Nano* **2010**, *4*, 2523−2530.
(46) Moon, G. D.; Min, Y.; Ko, S.; Kim, S.-W.; Ko, D.-H.; Jeong, U. Understanding the Epitaxial Growth of Se_xTe_y@Te Core-Shell Nanorods and the Generation of Periodic Defects. *ACS Nano* **2010**, *4*, 7283−7292.
(47) Yamauchi, T.; Tsukahara, Y.; Yamada, K.; Sakata, T.; Wada, Y. Nucleation and Growth of Magnetic Ni−Co (Core−Shell) Nanoparticles in a One-Pot Reaction under Microwave Irradiation. *Chem. Mater.* **2011**, *23*, 75−84.
(48) Radisavljevic, B.; Radenovic, A.; Brivio, J.; Giacometti, V.; Kis, A. Single-Layer MoS_2 Transistors. *Nat. Nanotechnol.* **2011**, *6*, 147−150.
(49) Min, Y.; Roh, J.; Yang, H.; Park, M.; Kim, S. I.; Hwang, S.; Lee, S. M.; Lee, K. H.; Jeong, U. Surfactant-Free Scalable Synthesis of Bi_2Te_3 and Bi_2Se_3 Nanoflakes and Enhanced Thermoelectric Properties of Their Nanocomposites. *Adv. Mater.* **2013**, *25*, 1425−1429.
(50) Min, Y.; Moon, G. D.; Kim, B. S.; Lim, B.; Jeong, U. Quick, Controlled Synthesis of Ultrathin Bi_2Se_3 Nanodiscs and Nanosheets. *J. Am. Chem. Soc.* **2012**, *134*, 2872−2875.